Mendeleev Communications

Mendeleev Commun., 2027, **37**, in press

Local structure of $Pr_5Mo_{2.7}O_{16-\delta}$ prepared by precursor technique: a Raman spectroscopy study

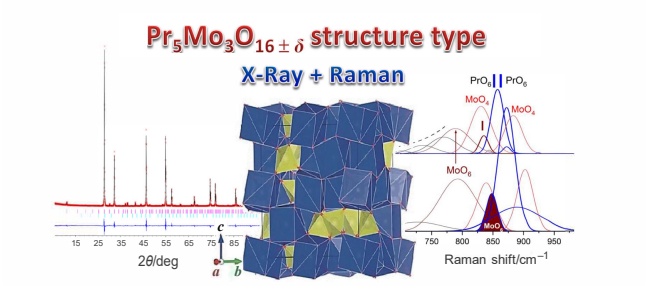
Sergey N. Shkerin,[a] Olga I. Gyrdasova,*[b] Rayana K. Abdurakhimova,[a] Liliya A. Pasechnik,[b] Alexandr Yu. Chufarov,[a] Sergey M. Beresnev,[a] Alexandr I. Balitskiy[b] and Mikhail V. Kuznetsov[b]

[a] *Institute of High-Temperature Electrochemistry, Ural Branch of the Russian Academy of Sciences, 620066 Ekaterinburg, Russian Federation*

[b] *Institute of Solid State Chemistry, Ural Branch of the Russian Academy of Sciences, 620077 Ekaterinburg, Russian Federation. E-mail: gyrdasova@ihim.uran.ru*

DOI: 10.71267/mencom.8100

Anion-deficient praseodymium molybdate $Pr_5Mo_{2.7}O_{16-\delta}$ with a fluorite-type structure was synthesized by carboxylate technique. Using Raman spectroscopy, the simultaneous presence of MoO_4 and MoO_6 polyhedra, as well as PrO_6 and PrO_8 polyhedra, was revealed for the first time in the $Pr_5Mo_{2.7}O_{16-\delta}$ structure. The predicted high ionic conductivity in these structures is due to the percolation network of MoO_4–MoO_6 polyhedra.



Keywords: praseodymium molybdate, crystal structure, Raman spectroscopy, precursor synthesis, molybdenum/praseodymium formate, paddle-wheel mechanism for ion transport.

Molybdenum-containing oxides crystallizing in perovskite and fluorite structures have been recently considered among the most promising electrode materials for symmetric solid oxide fuel cells. The advantage of molybdenum in such oxides is its ability to readily change its oxidation state under variations in the partial pressure of oxygen while maintaining the crystalline structure.[1] In addition, oxygen vacancies form quite easily in such structures. This ensures rapid transport of oxygen ions, which helps to increase the efficiency of the oxygen reduction reaction at the cathode.

Recently,[2] the cause of the high conductivity and instability of lanthanum molybdate was understood: a non-autonomous phase, $La_5Mo_3O_{16}$, with high transport properties forms at the interface between the $La_2Mo_2O_9$ and $La_2Mo_3O_{12}$ phases. Similar phases containing Nd or Pr are stable.[3–8] This has driven practical interest in the production and study of fluorite-like $Pr_5Mo_3O_{16-\delta}$ (PMO). PMOs were obtained *via* standard ceramic technique, which requires long sintering times, high temperatures, and often does not ensure true compositional homogeneity.[3,5–9] Considering that the practically significant properties of complex oxide materials (the degree of defectiveness, porosity, size and spatial morphology of crystallites) are determined by the synthesis method, it seems advisable to use solution methods to obtain $Pr_5Mo_3O_{16-\delta}$. These techniques allows one to control the concentration of target defects by reducing the synthesis temperature. For example, using the sol–gel method to produce single-phase neodymium molybdate $Nd_5Mo_3O_{16+\delta}$ reduces the synthesis temperature by 200 K.[7] The structure of the $Ln_5Mo_3O_{16+\delta}$ single crystals has been studied by X-ray diffraction (XRD) methods, high-resolution transmission electron microscopy (HRTEM), energy-dispersive X-ray spectroscopy (EDXS) microanalysis and X-ray absorption near edge structure (XANES) spectroscopy.[5–7] However, we did not find a single study on the local structure of these materials using Raman spectroscopy. The only work[9] that presents experimental data on Raman spectra refers to molybdates with a different cationic composition.

At the first stage of this study, samples of the known composition $Pr_5Mo_3O_{16-\delta}$ were synthesized using precursor methods. Analysis of X-ray diffraction patterns by the Rietveld method showed that, in addition to the phase with a fluorite-like structure and cubic symmetry (space group *Pn*3*n*, No. 222), a small amount of another cubic phase is always present in the material. The amount of the impurity phase decreases with reducing oxygen activity in the atmosphere during annealing or synthesis, but it is not possible to eliminate it completely. Based on our experience with oxide materials having a fluorite-type structure, we assumed that this impurity phase is related to molybdenum-rich regions. To test this hypothesis, a new composition with reduced molybdenum content ($Pr_5Mo_{2.7}O_{16-\delta}$) has been selected, which is presumably single-phase.

The aim of this study has been to develop new synthesis methods of the fluorite-like material of $Pr_5Mo_3O_{16-\delta}$ type and to investigate its composition and structure, including the local symmetry, using Raman scattering (for details, see Online Supplementary Materials). Two synthetic routes: a sol–gel method and a carboxylate precursor method, in which formic acid[10] was used as the carboxylic acid (Figures S1 and S2) were developed for the preparation of praseodymium molybdate $Pr_5Mo_{2.7}O_{16-\delta}$ (see Online Supplementary Materials).

XRD analysis shows that $Pr_5Mo_3O_{16-\delta}$ prepared by the formate method contains 95.4 wt% of the main fluorite-type phase (space group *Pn*3*n*) and only 4.6 wt% of $Pr_2Mo_2O_{8.66}$ impurity, whereas the sol–gel product has 12.5 wt% impurity (Figure S3). By synthesizing $Pr_5Mo_{2.7}O_{16-\delta}$ *via* the formate route, the impurity content is further reduced to 0.2 wt% (Figure 1). Refined crystallographic parameters are given in Tables S1 and S2.[6,7] These results demonstrate that the formate

© 2027 Mendeleev Communications

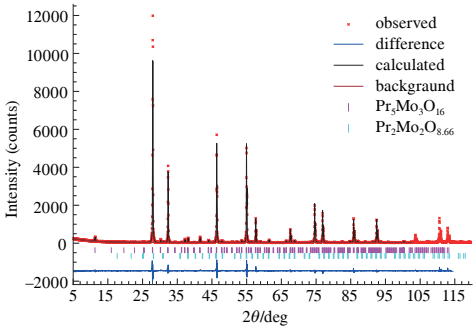


Figure 1 X-ray pattern of the $Pr_5Mo_{2.7}O_{16-\delta}$ obtained by formate method.

method is optimal for synthesizing the molybdenum-deficient $Pr_5Mo_{2.7}O_{16-\delta}$ composition. Therefore, all subsequent studies were conducted on the sample prepared by the formate route.

SEM study (Figure S4) reveals crystallisation of Pr and Mo formates as spherical aggregates and fibrous crystals, respectively. The thermolysis products Pr_6O_{11} and Mo_2O_3 inherit the precursor morphology (pseudomorphism). Agglomerates of $Pr_5Mo_{2.7}O_{16-\delta}$ are morphologically identical to Pr_6O_{11}, with uniform elemental distribution (see EDX in Figure S5).

According to the XRD data (Table S2), it is safe to assume the existence of only two allowed positions for Pr and Mo atoms. Indeed, the $Pr_5Mo_3O_{16\pm\delta}$ structure consists of edge-sharing PrO_8 polyhedra and vertex-sharing MoO_4 tetrahedra. Therefore, the MoO_4 tetrahedra in $Pr_5Mo_3O_{16}$ form a fairly compact and mobile structural unit, capable of migrating along the loose fluorite-like structure.[5–7] However, in some rare-earth molybdates, three types of molybdenum coordination were observed simultaneously: tetrahedral (MoO_4), trigonal-bipyramidal (MoO_5) and octahedral (MoO_6).[11,12] Neutron diffraction data for $Pr_5Mo_3O_{16\pm\delta}$ single crystals showed that Mo atoms in the main positions are surrounded by four oxygen atoms, while Mo atoms localized near the Pr positions are surrounded by six oxygen atoms.[6] Thus, a number of structural studies revealed a partial mutual substitution of Pr and Mo atoms in the Hubert structure.[5,6,11,12] The disorder of the oxygen sublattice, caused by the redistribution of Pr and Mo cations, ensures the continuity of the oxygen migration network. To clarify the local structural features of the $Pr_5Mo_{2.7}O_{16-\delta}$ sample obtained by the formate method, Raman spectroscopy was employed.

The Raman spectrum of $Pr_5Mo_{2.7}O_{16-\delta}$ [Figure 2(*a*)] differs strongly from that of pure fluorite which has only one line. To circumvent a strong photoluminescence background from anion vacancies complicating the spectrum,[13] we used anti-Stokes acquisition. The position of the structural lines does not depend on the laser wavelength, but the luminescence lines shift significantly. The anti-Stokes intensity decays exponentially (Figure S6), allowing reconstruction of pure structural Raman lines. Spectra obtained by the anti-Stokes method contain only structural modes. They were distinguished into a set of Gaussian lines using the Peak Separation 2 package. An example of decomposition is shown in Figure 2(*b*). Deconvolution into Gaussian components yields the spectra shown in Figures 2(*c*) and (*d*) for samples annealed in air and argon.

The application of this approach to the study of praseodymium molybdate proved difficult because of the complex nature of the spectrum. Therefore, we developed an alternative method for reliable identification of structural lines.[14] When an electromagnetic wave of frequency f_0 hits a set of charges, they begin to vibrate, utilizing the incident energy. Of all possible frequencies, the strongest amplitudes will be observed for the frequencies of natural vibrations of the charge system φ_k. Because of inelastic scattering, a network of vibrations with frequencies appears: $f_0 + \varphi_k$ and $f_0 - \varphi_k$, for k = 1…N.

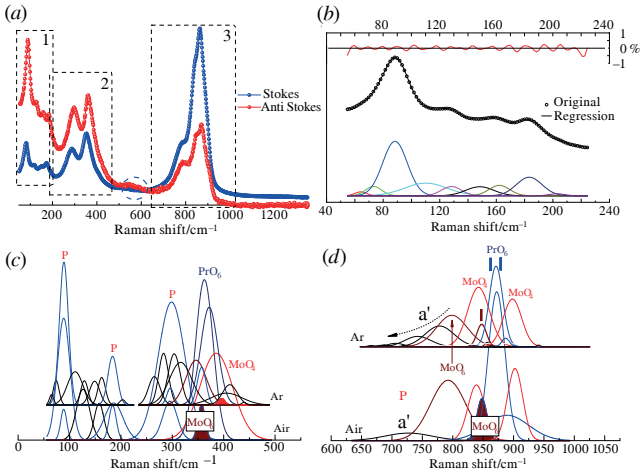


Figure 2 (*a*) Stokes and anti-Stokes Raman spectra ($\lambda = 532$ nm) of $Pr_5Mo_{2.7}O_{16-\delta}$; (*b*) representative Gaussian fitting of the experimental curve; (*c*), (*d*) deconvolution of the Raman spectrum into individual Gaussian components.

Lines at 88, 183, 299, 357, 847, 871 and 888 cm^{-1} are independent of oxygen activity, while others shift by ~10 cm^{-1} with oxygen activity (362–370, 792–799, 839–843 and 902–898 cm^{-1}). The three low-frequency lines (88, 183 and 299 cm^{-1}) are assigned to the pyrochlore structure which is marked as 'P' in Figures 2(*c*) and 2(*d*).[15] For classical fluorite, only one F_{2g} mode would appear, but local symmetry lowering to pyrochlore is typical for cation-disordered fluorites.[13] Molybdenum in molybdates can be four- or six-coordinated (Table S3). Comparison with the known Raman spectra of MoO_4[16] (Table S4) shows good agreement for the three lines highlighted in red in Figures 2(*c*) and 2(*d*). The disappearance of the mode at 933 cm^{-1} indicates the absence of distortions in the tetrahedra (a decrease in the polarizability of MoO_4). The asymmetric vibrational modes retain their Raman activity. According to the Raman spectra, the sample is a fluorite-type solid solution with a random cation distribution. The high concentration of oxygen vacancies promotes the formation of highly symmetrical MoO_4 polyhedra. Only the combination of XRD (long-range) and Raman (short-range) provides this insight.

Literature data for MoO_6 (Table S5) allow assignment of lines at 356, 847 cm^{-1} (oxygen-independent) and 793/798 cm^{-1} (forming satellites under reducing conditions). Two intense lines at 887 and 871 cm^{-1} and those at 372 and 362 cm^{-1} are related to the PrO_6 polyhedron – the first such assignment. Pr^{4+} in PrO_6 is not known; these correspond to Pr^{3+}.[17] Very weak lines [blue circle in Figure 2(*a*)] may also arise from Pr^{3+} polyhedra. External lattice vibrations are a superposition of librational and translational modes.[9] The 88, 183 and 299 cm^{-1} modes (pyrochlore) do not depend on oxygen activity. The diffuse band near 726 cm^{-1} (air-annealed sample) corresponds to the F_{2g} pyrochlore mode; its oxygen-pressure sensitivity confirms the assignment. The 299 cm^{-1} mode weakens and develops satellites in argon, indicating dynamic disorder.

Pyrochlore is built of MeO_8 polyhedra. Only Pr can form such polyhedra (Table S3). It should be taken into account that the MoO_6 and MoO_4 polyhedra are smaller than the basic polyhedra of the PrO_8 lattice, which results in the 'loosening' of Mo-containing polyhedra. For such loose polyhedra, anion transport can occur *via* rotation around the central cation – the paddle-wheel mechanism – with significantly lower activation energy than vacancy hopping. Therefore, oxygen ion transport through the MoO_6–MoO_4 percolation network allows one to predict the high ionic conductivity of these molybdates.[5–18]

The nominal composition $Pr_5Mo_{2.7}O_{16-\delta}$ suggests a mixed valence state for Mo as $Mo^{5+/6+}$ and Pr as $Pr^{3+/4+}$.[19] To clarify the

actual valence states, X-ray photoelectron spectroscopy (XPS) was used. The survey spectrum [Figure 3(*a*)] reveals peaks for Pr, Mo, O and C, as well as Auger features. The C1*s* peak at 284.5 eV from adsorbed carbon served for charge referencing. The Pr3*d* spectrum [Figure 3(*b*)] displays two main peaks at 932.6 eV (Pr3$d_{5/2}$) and 952.1 eV (Pr3$d_{3/2}$). The spin–orbit splitting of 20.5 eV and the satellite structure indicate Pr^{3+}.[20] Although the XPS signatures of PrO_2 and Pr_2O_3 are similar, making it difficult to distinguish Pr^{3+} from Pr^{4+} when both are present,[18,19] no characteristic features of Pr^{4+} are observed, implying that the surface is predominantly trivalent.

The Mo3*d* spectrum [Figure 3(*c*)] consists of a doublet at 232.3 eV (Mo3$d_{5/2}$) and 235.4 eV (Mo3$d_{3/2}$) which matches Mo^{6+}.[20] Signals from Mo^{5+} or Mo^{4+} are absent. Consequently, XPS confirms the nominal composition – praseodymium oxide doped with Mo^{6+}, with praseodymium mainly in the Pr^{3+} state on the surface.

Thus, the possibility of obtaining a new single-phase $Pr_5Mo_{2.7}O_{16-\delta}$ using precursor technique has been demonstrated and realised. The chemical composition of the material – praseodymium oxide doped with molybdenum – was confirmed by XPS, which shows that praseodymium in the surface layers is in the ground state Pr^{3+} and molybdenum is present as Mo^{6+}. Raman scattering spectra were studied using an improved method that eliminates the contamination of structural lines by photoluminescence from intrinsic defects (oxygen vacancies). Comparison with literature data allowed us to assign the observed lines to the MoO_4 and MoO_6 polyhedra. A set of high-intensity lines, similar to that of the MoO_6 polyhedron, is assigned to the PrO_6 polyhedron. The lattice is based on a pyrochlore-type structure built from PrO_8 polyhedra. Molybdenum cations accumulate oxygen vacancies in their environment, forming a network of MoO_4 and MoO_6 polyhedra. The transport of oxygen anions through the MoO_6–MoO_4 percolation network can provide high anionic conductivity for this type of molybdate. The existence of PrO_6 polyhedra is noteworthy, as it indicates that Pr-containing polyhedra are also involved in stabilizing MoO_4 polyhedra. The set of Raman lines for this polyhedron is reported for the first time.

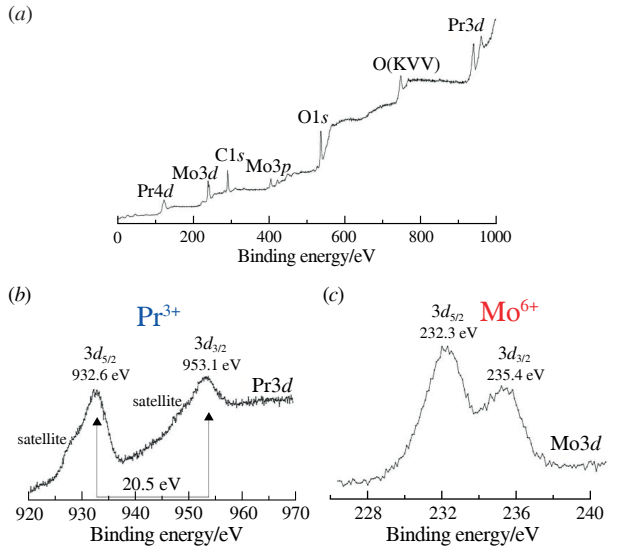


Figure 3 XPS-spectrum for $Pr_5Mo_{2.7}O_{16-\delta}$ samples: (*a*) overview and core electronic levels for (*b*) Pr3*d* and (*c*) Mo3*d*.

This work was carried out in accordance with the state assignment and research plans of IHTE UB RAS and ISSC UB RAS.

Online Supplementary Materials

Supplementary data associated with this article can be found in the online version at doi: 10.71267/mencom.8100.

References

1 P. Lacorre, F. Goutenoire, O. Bohnke, R. Retoux and Y. Laligant, *Nature*, 2000, **404**, 856; https://doi.org/10.1038/35009069.
2 N. Porotnikova, A. Khrustov, A. Farlenkov, A. Khodimchuk, G. Partin, I. Animitsa, N. Kochetova, D. Pavlov and M. Ananyev, *ACS Appl. Mater. Interfaces*, 2022, **14**, 6180; https://doi.org/10.1021/acsami.1c20839.
3 V. I. Voronkova, I. A. Leonidov, E. P. Kharitonova, D. A. Belov, M. V. Patrakeev, O. N. Leonidova and V. L. Kozhevnikov, *J. Alloys Compd*., 2014, **615**, 395; https://doi.org/10.1016/j.jallcom.2014.07.019.
4 E. I. Get'man, K. A. Chebyshev, L. V. Pasechnik, L. I. Ardanova, N. I. Selikova and S. V. Radio, *J. Alloys Compd*., 2016, **686**, 90; https://doi.org/10.1016/j.jallcom.2016.06.005.
5 K. A. Chebyshev, T. S. Berezhnaya and V. A. Turchenko, *Solid State Sci.*, 2024,**149**,107443; https://doi.org/10.1016/j.solidstatesciences.2024.107443.
6 A. M. Antipin, O. A. Alekseeva, N. I. Sorokina, A. N. Kuskova, V. V. Artemov, V. Yu. Murzin, E. P. Kharitonova, E. A. Orlova and V. I. Voronkova, *Crystallogr. Rep*., 2015, **60**, 640; https://doi.org/10.1134/S1063774515050028.
7 M. J. Martinez-Lope, J. A. Alonso, D. Sheptyakov and V. Pomjakushin, *J. Solid State Chem*., 2010, **183**, 2974; https://doi.org/10.1016/j.jssc.2010.10.015.
8 N. V. Lyskov, A. I. Kotova, D. I. Petukhov, S. Ya. Istomin and G. N. Mazo, *Russ. J. Electrochem.*, 2022, **58**, 989; https://doi.org/10.1134/S102319352211009X.
9 A. V. Shlyakhtina, N. V. Lyskov, I. V. Kolbanev, A. N. Shchegolikhin, O. K. Karyagina and L. G. Shcherbakova, *Int. J. Hydrogen Energy*, 2021, **46**, 16989; https://doi.org/10.1016/j.ijhydene.2021.01.129.
10 O. I. Gyrdasova, R. F. Samigullina, E. V. Vladimirova, I. S. Medyankina, L. Yu. Buldakova, M. Yu. Yanchenko and L. A. Pasechnik, *Mendeleev Commun.*, 2024, **34**, 640; https://doi.org/10.1016/j.mencom.2024.09.005.
11 I. Radosavljevic Evans, J. A. K. Howard and J. S. O. Evans, *Chem. Mater*., 2005, **17**, 4074; https://doi.org/10.1021/cm050049+.
12 D. Schildhammer, G. Fuhrmann, L. Petschnig, M. Kogler, S. Penner, N. Weinberger, H. Schottenberger and H. Huppertz, *Solid State Sci.*, 2016, **62**, 22; http://doi.org/10.1016/j.solidstatesciences.2016.10.011.
13 S. N. Shkerin, E. S. Ul'yanova and E. G. Vovkotrub, *Inorg. Mater*., 2021, **57**, 1145; https://doi.org/10.1134/S0020168521100137.
14 S. N. Shkerin and R. K. Abdurakhimova, *Patent RU* 2849022 C1, 2025; https://patents.google.com/patent/RU2849022C1/en?oq=Patent+RU+2849022.
15 V. A. Chernyshev, *Phys. Solid State*, 2021, **63**, 953; https://doi.org/10.1134/S1063783421070040.
16 M. Wang, C. Wang, J. Wang, L. Lu, X. Gong, X. Tang, F. Zhang and J. You, *Materials,* 2020, **13**, 5453; https://doi.org/10.3390/ma13235453.
17 M. V. Abrashev, N. D. Todorov and J. Geshev, *J. Appl. Phys*., 2014, **116**, 103508; https://doi.org/10.1063/1.4894775.
18 H. He, H. X. Dai, K. W. Wong and C. T. Au, *Appl. Catal.*, 2003, **251**, 61; https://doi.org/10.1016/S0926-860X(03)00309-0.
19 E. Poggio-Fraccari, G. Baronetti and F. Mariño, *J. Electron Spectrosc. Relat. Phenom.*, 2018, **222**, 1; https://doi.org/10.1016/j.elspec.2017.11.003.
20 F. Xie, W. C. H. Choy, C. Wang, X. Li, S. Zhang and J. Hou, *Adv. Mater*., 2013, **25**, 2051; https://doi.org/10.1002/adma.201204425.

Received: 19th May 2026; Com. 26/8100

Mendeleev Commun., 2027, **37**, in press

Contents entry

Local structure of $Pr_5Mo_{2.7}O_{16-\delta}$ prepared by precursor technique: a Raman spectroscopy study

Sergey N. Shkerin, Olga I. Gyrdasova, Rayana K. Abdurakhimova, Liliya A. Pasechnik, Alexandr Yu. Chufarov, Sergey M. Beresnev, Alexandr I. Balitskiy, Mikhail V. Kuznetsov

